*Acta Oceanol. Sin.*, 2017, Vol. 36, No. 5, P. 44–50
DOI: 10.1007/s13131-017-1059-2
http://www.hyxb.org.cn
E-mail: hyxbe@263.net

# A study on the relationships between the wave height and the El Niño in the north area of the South China Sea

HAN Shuzong[1]*, FAN Yongbin[1], DONG Yangyang[1], WU Shuangquan[2]

[1] College of Oceanic and Atmospheric Sciences, Ocean University of China, Qingdao 266100, China

[2] National Marine Information Center, State Oceanic Administration, Tianjin 300171, China

Received 7 June 2016; accepted 16 September 2016



**Abstract**

On the basis of the European Centre for Medium-range Weather Forecasts (ECMWF) 20 a wind field reanalysis data, the wave field of the north area of the South China Sea is calculated with the combination of the HIRHAM wind field model and the SWAN wave model. Then a significant wave height compared with the El Niño index to study the relationships between these variables. The following conclusions are drawn: (1) the wave height of the South China Sea has a strong seasonal variation, the wave height is much larger in winter than in summer; (2) in the South China Sea, the monthly average wave height of the north area has a negative correlation with the Niño3.4 index, most area of the South China Sea has a moderate correlation and the area between Taiwan Province of China and Philippines is highly correlated; and (3) in the strong El Niño years, the significant wave height in the north area of the South China Sea is significantly smaller than in other years; if the El Niño index variability is greater, the wave height decreases. In contrast, the significant wave height in the north area of the South China Sea is larger in the strong La Niña years.

**Key words:** South China Sea, SWAN, wave, significant wave height, El Niño

**Citation:** Han Shuzong, Fan Yongbin, Dong Yangyang, Wu Shuangquan. 2017. A study on the relationships between the wave height and the El Niño in the north area of the South China Sea. Acta Oceanologica Sinica, 36(5): 44–50, doi: 10.1007/s13131-017-1059-2

## 1 Introduction

Sea wave is a small-scale surface gravity wave generated by the wind. The forecast and the hindcasting of the sea wave are a major focus of physical marine research. As a key area of our national future ocean development, the calculation and research of wave elements in the South China Sea are important. To date, there has been substantial research into the South China Sea waves and the majority of these studies fit into three categories (Zhou et al., 2007); the first of these focuses on the analysis of actual measured field data and draws the conclusions based on these analyses. According to the typhoon wind field materials and wave observation results from the South China Sea in 1964–1987, Chen (1989) concluded the typhoon wave distribution and wave height laws of the South China Sea. On the basis of the materials in the ship weather report, Zhuang (1999) analyzed the characteristics of the typhoon field and wave field of the northwest Pacific Ocean. Yu (1984) analyzed the distribution characteristics of the South China Sea wave based on the ship materials. Yang et al. (2015) studied the typhoon wave spectrum in the northern South China Sea using the data measured in 2010 by a wave rider buoy.

While the analysis of the actual measured method is constrained to the actual field measurement data; the second type of study has focused on the reanalysis data from remote sensing materials such as satellites. Using the GEOSAT satellite altimeter materials, Qi et al. (1998a, b) analyzed the wave characteristics of the north area of the South China Sea and produced the statistical analyses of the surface wind speed and wave characteristics in the process of the No. 8708 typhoon. Wan et al. (2015) assessed the wave energy resources in China's seas based on multi-satellite merged radar altimeter data. Yaakob et al. (2016) presented an assessment of the wave energy resources in the South China Sea (Malaysian exclusive economic zone) using a satellite altimeter.

There are many processing errors that can occur when dealing with wind processing by satellite altimeter materials; therefore, the third type of study of the South China Sea applies forecast and hindcasting based on numerical models. Zhou et al. (2007) produced an analysis of the wave field of the South China Sea using the WAVEWATCH III model. Jiang et al. (2011) produced a comparison analysis of the wave simulation results of the north area of the South China Sea using the WAVEWATCH III and SWAN models. Using the SWAN model, Zheng et al. (2011) examined the wave energy resources of the north area of the South China Sea. Zheng et al. (2013) assessed the China's seas wind energy and wave energy resources from 1988 to 2009 using WAVEWATCH III, with a cross-calibrated, multi-platform (CCMP) wind field as the driving field. With the development of numerical model technology, numerical models have become widely applied by physical oceanography scholars.

In this study, we used a numerical model to simulate the wave field in the northern part of the South China Sea. We also explored El Niño's influence on the wave height of the north area of the South China Sea and between these variables.

## 2 Introduction to the numerical model

In this study, based on the European Centre for Medium-range Weather Forecasts (ECMWF) years' highly precise global

*Corresponding author, E-mail: hansz@ouc.edu.cn

reanalysis of the wind field, we used the HIRHAM wind field model and the SWAN (simulating waves nearshore) wave model, which has been applied and verified in many waters worldwide to calculate the wave field of the South China Sea. We use these models to make a comparison between the wave height results and the El Niño phenomenon to explore the influence of El Niño on the wave heights of the north area of the South China Sea.

### 2.1 *Sea surface wind field numerical model*

This paper concerns the scope of the northern area of the South China Sea (15°–25°N, 105°–125°E), as shown in Fig. 1. This area has a tropical and subtropical climate, and the synoptic system is controlled by the large-scale circulation of the Qinghai–Tibet Plateau, the equatorial Pacific Ocean and the East Asia temperate zone. The extreme weather events at sea include typhoon, cold wave, typhoon and cold wave, extratropical cyclones and mesoscale processes.

The numerical calculation of the wave is strongly influenced by the wind field. The global reanalysis of the wind field by the ECMWF is generally the world's best global reanalysis product. However, when applied to environmental engineering research in China's coastal waters, it becomes apparent that its temporal and spatial resolution require improvement. This is associated with the low simulated intensity of the extreme weather events (typhoons, cold waves, extratropical cyclones and mesoscale processes). Therefore, we adopted the hindcasting model HIRHAM at high resolution to improve the simulation of the gale accidents such as cold waves and extratropical cyclones. We also use the hybrid wind field and the typhoon model wind field to improve the simulation of the typhoon events.

In this study, we used the global reanalysis wind field of the ECMWF as boundary conditions for the HIRHAM model. This product uses the IFS Cy31r1/2 version of the latest European center atmospheric model, adopting the four-dimensional variation assimilation technology (4DVAR) and has 60 vertical levels. In addition to assimilating all the traditional satellites and ground observations, many other data sources have also been assimilated, including the new ERS (European remote sensing satellite) altimeter wave data, wind and clear sky radiation dates of the satellite reprocessed by EUMETSAT (European Organization for the Exploitation of Meteorological Satellites), GOME (global ozone monitoring experiment) ozone data and GPS data from CHAMP (challenging minisatellite payload), GRACE (gravity recovery and climate experiment) and COSMIC (constellation observing system for meteorology, ionosphere and climate).

The HIRHAM is a northern European weather hindcasting pattern. The development of this pattern integrates the advantages of two European regions and global atmospheric general circulation models: HIRLAM and ECHAM. The weather forecast model of the HIRLAM high resolution model is a business numerical forecast model jointly developed by several European countries. The HIRLAM model is today used in the weather bureaus of Denmark, Finland, Iceland, the Netherlands, Norway, Spain and Sweden, and represents an advanced level of numerical prediction in international areas. The ECHAM model, developed by Germany's Max Planck Institute of Meteorology, is a global atmospheric general circulation model. The HIRHAM uses the dynamic framework of the HIRLAM model and the physical parameterization scheme of the ECHAM. The model was jointly developed by Danish Weather Bureau and Germany's Max Planck Institute for Meteorology. In recent years, the HIRHAM has been widely used in a regional climate change numerical simulation and a high resolution reanalysis research focusing on regions including Europe, Greenland, Antarctica and central Asia.

### 2.2 *Wave field model*

The SWAN model is the third generation wave numerical model developed by the Delft University in the Netherlands. This model applies one of the most widely used and mature patterns. This model solves the spectrum action balance equation under a condition in which the wave growth spectral pattern is not limited in advance.

The basic principle of the SWAN is similar to that of the WAM Cycle 3. However, the WAM model has mainly been applied at the ocean scale, and the SWAN, which can obtain the ideal wave parameter estimation if given the wind field, the water depth, the flow field and boundary conditions, is applied to coasts, lakes

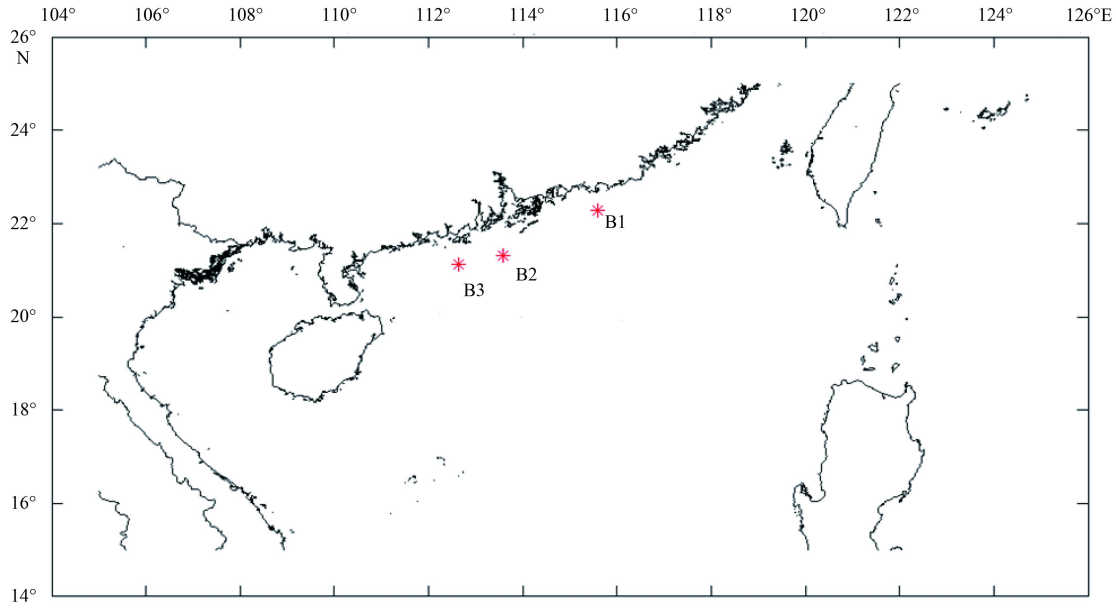


**Fig. 1.** Map of the study area indicating the positions of the verification point sites.

and estuaries. Compared with other wave models, the advantages of the SWAN model are as follows: first, it is very stable under any conditions; and second, closed boundary conditions are not required. However, the SWAN model also has its limitations: first, it cannot calculate the wave-induced current under the two-dimensional case, thus the increased water caused by waves should be approximated; second, it is not suitable for calculating the diffraction within one or two wavelength coverage behind the top of obstacles and not suitable for simulating harbor waves for which the diffraction effect is very strong. After a great deal of inspection of many forecasts and hindcasts under all kinds of weather conditions, this model was submitted to the marine forecast center of the State Oceanic Administration. The results have shown that the stability, applicability and precision of this model are strong (Han and Shi, 2013).

In this paper, the SWAN model selected the rules grid and used the non-static mode in a spherical coordinate system. The discretization method of the time and space was in S&L format, the spatial resolution of the model was 0.125°×0.125°, and the computation time step was 30 min. The spatial resolution of the terrain data was 1′×1′. The spatial resolution of the wind field was 0.125°×0.125°. In the physical mechanism of the model, the wind energy input considered both linear and exponential growth (linear growth was described using the Caraler and Malanotte-Rizzoli formula and exponential growth was described using the Komen proposed empirical formula). In addition, we corrected the wind energy input according to the methods of Jia et al. (2010). Other parameters of the model were set as default values.

In the SWAN model, the land boundary absorbs the wave energy completely and the wave has free access in the deep boundary. Under normal conditions, it is difficult to obtain the initial wave field in the calculation area. In this paper, we set the initial state of the calculation to select the ideal quiet plane. In order to minimize the effect of the initial field, the model calculated 2 d earlier than the actual calculation of the time.

## 3 Data specification

### 3.1 *Wind field input*

The wind field used in this article was based on the global reanalysis wind field of the ECMWF, obtained by using the HIRHAM model to improve the simulation of the cold wave, cyclone and other gale events. The time period was from 00:00 of January 1, 1993 to 18:00 on December 31, 2012, four times a day (6 h), and 20 a in total. The spatial resolution was 0.125°×0.125°.

### 3.2 *Terrain data*

The terrain data used the ETOP01 and the spatial resolution is 1′×1′.

### 3.3 *Verified wind and wave field data*

This study verified the effects of the wind speed, the wind direction, the significant wave height, the wave cycle, the wave direction on the hindcast result of the wind field model and the calculated wave results. All the above data were measured with a 10 m diameter buoy system, which was released by the South China Sea Branch of the State Oceanic Administration in January 2010.

## 4 Verification of simulated results

### 4.1 *Verification of the results of the wind field model*

We selected the measured data of three South China Sea buoys to verify the calculation results of the wind field (their positions are shown in Fig. 1). The three buoy stations are respectively described as B1, B2 and B3 (measured by the State Oceanic Administration 10 m diameter buoy system). The main observation elements include the significant wave height, the period, the wave direction, the wind speed and the wind direction. In this study, we compared the buoy wind speed data and the reanalysis wind speed data. The time intervals were 6 h and a total of 1 460 data points were compared each year. The verification period of the measured data was between 2010 and 2012. The verification results are presented in Fig. 2. In addition, we calculated a mean absolute error, a root mean square error and a correlation coefficient (Table 1). These results indicate that the simulation results of the wind field are basically identical to the observation data.

### 4.2 *Verification result of the wave field model*

In order to verify the results of the SWAN wave field, we used the measured wave data of three buoyage systems positioned by the South China Sea Branch of the State Oceanic Administration in January 2010. The three buoys are B1, B2 and B3 respectively. The main observation factors are the significant wave height, the period, the wave direction, the wind speed and the wind direction. In this study, we compare the significant wave height data from the buoys and the model results (time intervals are 6 h and a total of 1 460 data points are compared each year). The measured time period for verification includes three years (2010, 2011 and 2012). The mean absolute error, the root-mean-square error and the correlation coefficient between the observations and the simulations were calculated and the results are presented in Table 2. Table 2 shows that the simulation results and the measured materials are basically consistent with few errors. On the basis of a comparison with the previous results, we found that the distribution characteristics of the wave height in this paper are consistent with previous studies (Zheng et al., 2013; Zheng and Li, 2015; Stopa et al., 2013).

## 5 Influence of El Niño on the wave height

The El Niño refers to the phenomenon whereby the water temperature in equatorial East Pacific rises abnormally, affecting thousands of kilometers. According to research by Feng (2001), Shi and Zhou (1990), Sun and Zhang (2007) and other previous scholars, we knew that on the occurrence year of El Niño, few tropical cyclones influence China. In contrast, before and after the occurrence year, tropical cyclones affect China with a higher frequency. Li (1988) shows that typhoon activities are closely related to El Niño; the annual average number of typhoons over the South China Sea is less than normal in El Niño year and greater in the La Niña year. Lim and Kim (2007) shows that the monsoon strength over Indonesia, including the maritime continent, and Northeast Asia, is weaker than normal in El Niño years. Waves are mainly influenced by the wind, so the height of wave will be affected by El Niño. In order to explore the influence of El Niño on the wave height of the South China Sea, we analyzed the wave features of the northern South China Sea from 1990 to 2012.

According to the wave field of the South China Sea computed by the SWAN model, we analyzed the wave height data and obtained a monthly average wave height from 1991 to 2012. Through the application of several years of monthly average El Niño index from the National Centers Environmental Prediction (NCEP) data, we obtained the correlation between the monthly average wave height anomaly and the Niño3.4 index. The distribution of the correlation coefficient is shown in Fig. 3.

Figure 3 demonstrates a negative correlation between the significant wave height in the northern South China Sea and the El

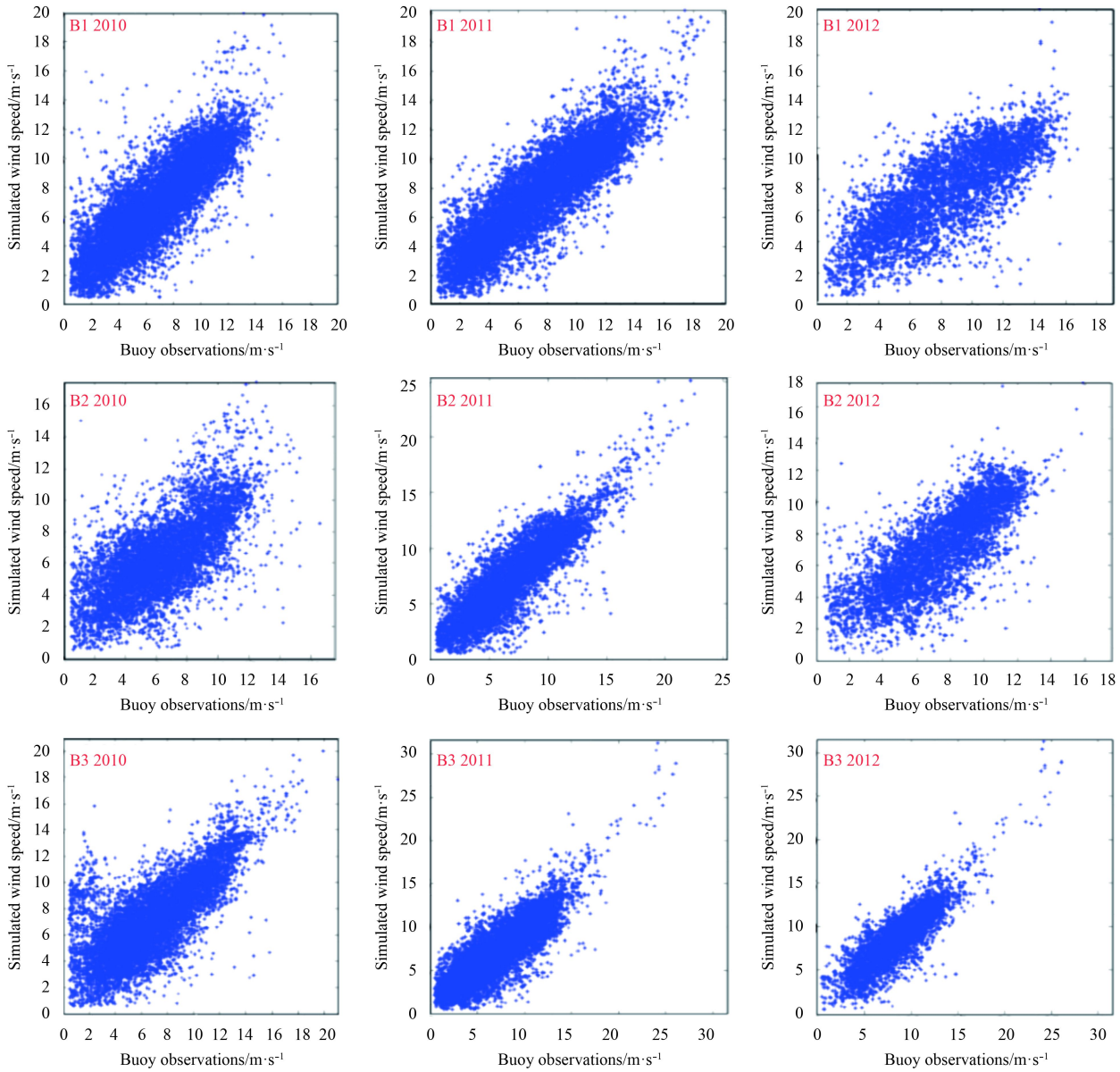


**Fig. 2.** Scatter diagrams of buoy observational and model simulated wind speeds.

**Table 1.** Verification results of comparing the simulated wind field and observational buoy data

| Buoy | Year | Mean absolute error/m·s$^{-1}$ | Root-mean-square error/m·s$^{-1}$ | Correlation coefficient |
|---|---|---|---|---|
| B1 | 2010 | 1.42 | 1.89 | 0.81 |
| B1 | 2011 | 1.38 | 1.78 | 0.87 |
| B1 | 2012 | 1.68 | 1.97 | 0.76 |
| B2 | 2010 | 1.66 | 1.89 | 0.68 |
| B2 | 2011 | 1.29 | 1.74 | 0.88 |
| B2 | 2012 | 1.45 | 1.92 | 0.76 |
| B3 | 2010 | 1.65 | 1.90 | 0.74 |
| B3 | 2011 | 1.37 | 1.83 | 0.85 |
| B3 | 2012 | 1.30 | 1.72 | 0.85 |

**Table 2.** Comparative verification result (observed vs simulated) for the wave field

| Buoy | Year | Mean absolute error/m | Root-mean-square error/m | Correlation coefficient |
|---|---|---|---|---|
| B1 | 2010 | 0.35 | 0.41 | 0.86 |
| B1 | 2011 | 0.31 | 0.39 | 0.88 |
| B1 | 2012 | 0.39 | 0.44 | 0.84 |
| B2 | 2010 | 0.38 | 0.46 | 0.84 |
| B2 | 2011 | 0.29 | 0.33 | 0.85 |
| B2 | 2012 | 0.36 | 0.45 | 0.89 |
| B3 | 2010 | 0.42 | 0.48 | 0.86 |
| B3 | 2011 | 0.38 | 0.46 | 0.87 |
| B3 | 2012 | 0.40 | 0.47 | 0.87 |

Niño index, a moderate correlation in most waters, and a high correlation in the strait between Taiwan Province of China and the Philippines.

In order to further explore the relation between the monthly average wave height and the Niño3.4 index, we produced an average distribution of the significant wave height in waters with high correlation. We then compared the monthly average significant wave height with the Niño3.4 regional abnormal index of the sea surface temperature. Its changes over time are presented in Fig. 4.

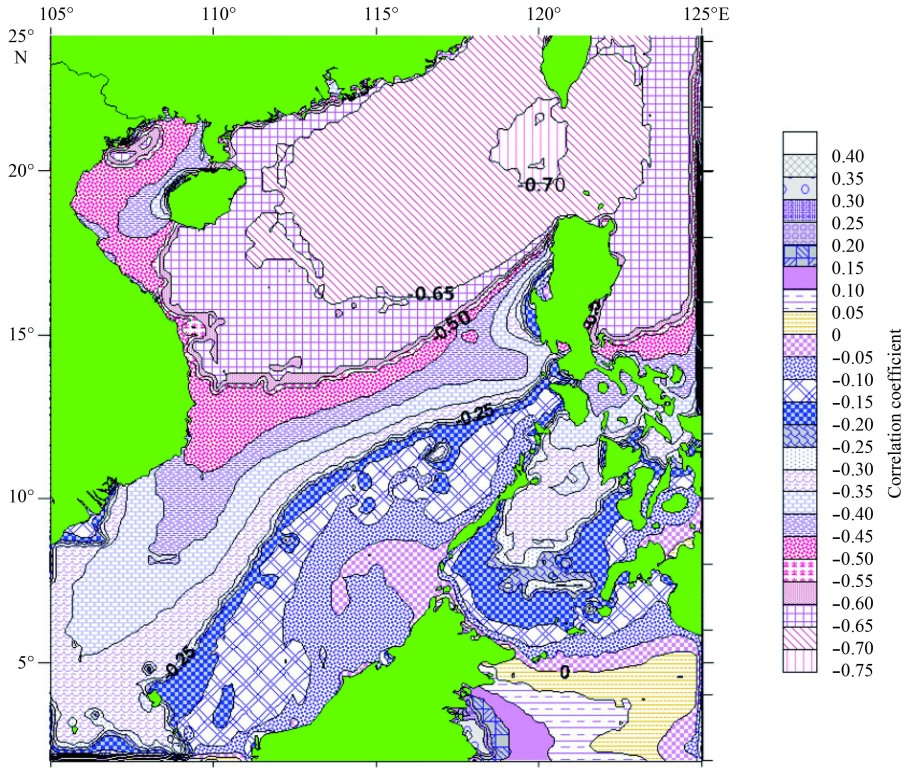


**Fig. 3.** Distribution diagram of the correlation coefficient of the monthly average wave height anomaly and the Niño3.4 index.

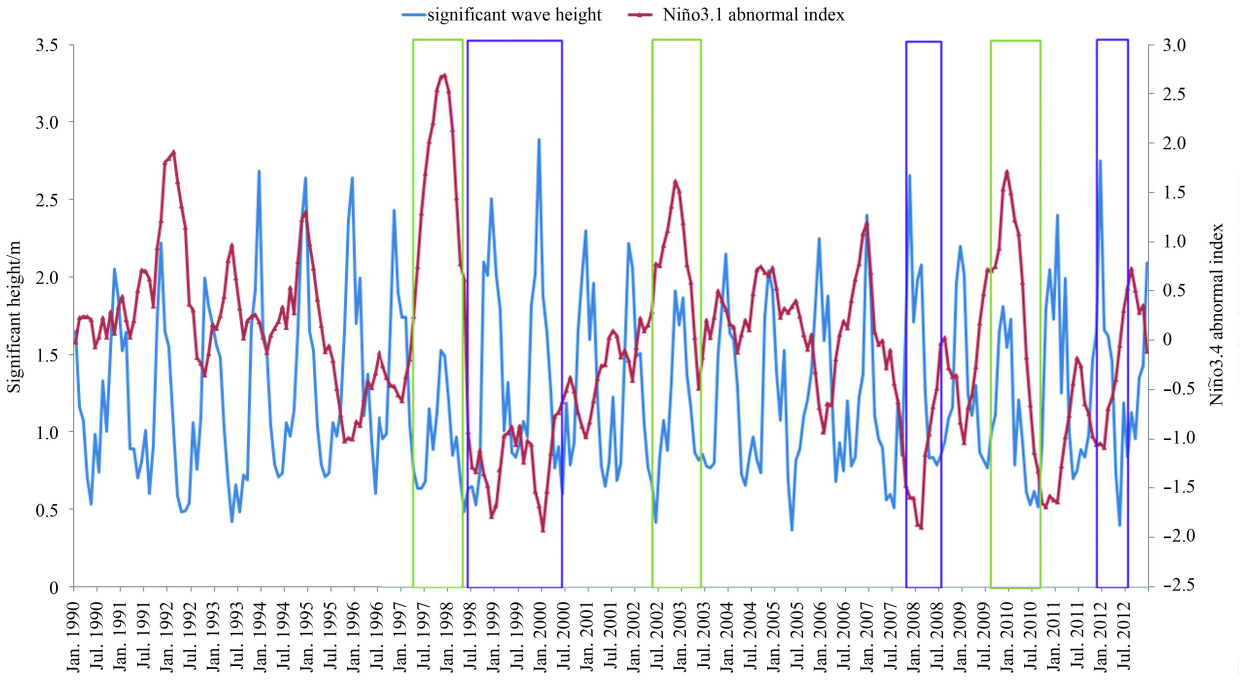


**Fig. 4.** Time-sequence variation diagram of the monthly average significant wave height with the Niño3.4 abnormal index of the sea surface temperature.

Figure 4 shows that the regional significant wave height demonstrates clear seasonal characteristics (the wave height in winter is higher than that in summer). This is consistent with the findings of previous research (Jiang et al., 2011; Zhou et al., 2007; Mirzaei et al., 2014).

Referring to related materials and articles and determining the monthly average sea temperature anomaly of the equatorial east Pacific as the index, we conclude that when the monthly average sea temperature anomaly is equal or greater than 0.5°C and lasts for at least half of the year, it is an El Niño event. Conversely, when the monthly average sea temperature anomaly is equal or less than 0.5°C and lasts for at least 0.5 a, a La Niña event may be assumed (Meng and Xu, 2007).

In order to explore the relationship between El Niño and the

wave height, we specifically focused on the strong El Niño years of 1997, 2002 and 2009 (Yuan et al., 2012), in which the El Niño index experienced great changes. Figure 4 shows that in strong El Niño years (green boxes), the regional significant wave height is apparently smaller; moreover, the greater the El Niño index changes, the smaller the wave height. In contrast, the regional significant wave height is greater in strong La Niña years (purple boxes).

## 6 Analysis of the mechanisms behind El Niño's influence on wave height

The main factors that influence the wave height are wind and topography. Through analyzing the relationship between the surface winds and the El Niño, Fang et al. (2006) found that El Niño highly influenced the wind. By looking up related materials and articles, we found that in El Niño years, the number of typhoons in the South China Sea strongly decreased and their intensity also reduced. While before and after the year of El Niño (always the year of La Niña), the frequency and intensity of typhoons apparently increased, causing a greater significant wave height (Chu and Cheng, 2008; Rogers et al., 2007; Kiladis and van Loon, 1988; Yadav et al., 2013). In addition, the monsoon is the main factor influencing the wave height in the South China Sea. The El Niño influences the occurrence time and the intensity of the monsoon, which produces impacts on the wave height of the region. Mirzaei et al. (2013) show that the significant wave height is negatively correlated with the Niño3.4 index during winter, spring and autumn seasons but became positive in the summer monsoon. Such correlations correspond well to surface wind anomalies over the South China Sea during El Niño events (Mirzaei et al., 2013).

## 7 Conclusions

(1) The wave height of the South China Sea shows a strong seasonal variation. The wave height in winter is higher than that in summer.

(2) There is a negative correlation between the monthly average wave height in the northern South China Sea and El Niño index, a moderate correlation in most waters, and a high correlation in the strait between Taiwan Province of China and the Philippines.

(3) The significant wave height in the northern South China Sea is apparently smaller in strong El Niño years; the greater the El Niño index changes, the smaller the wave height. In contrast, the significant wave height in the northern South China Sea is greater in strong La Niña years.

*Acknowledgements*

The authors thank the ECMWF for providing the sea surface wind speed data. We would also like to thank the NOAA National Weather Service Climate Prediction Center for providing the Niño3.4 index.

## References

Chen Qili. 1989. A study of typhoon waves in the South China Sea. Marine Forecasts (in Chinese), 6(3): 1–11

Chu P C, Cheng K F. 2008. South China Sea wave characteristics during typhoon Muifa passage in winter 2004. Journal of Oceanography, 64(1): 1–21

Fang Guohong, Chen Haiying, Wei Zexun, et al. 2006. Trends and interannual variability of the South China Sea surface winds, surface height, and surface temperature in the recent decade. Journal of Geophysical Research, 111(C11): C11S16

Feng Lihua. 2001. Tropical cyclone in China and El Niño event. Marine Science (in Chinese), 25(9): 36–38

Han Shuzong, Shi Yujiao. 2013. The distributional character of typhoon waves in the east China sea. Periodical of Ocean University of China (in Chinese), 43(10): 1–7

Jia Xiao, Pan Junning, Niclasen B. 2010. Improvement and validation of wind energy input in SWAN model. Journal of Hohai University: Natural Sciences (in Chinese), 38(5): 585–591

Jiang Lifang, Zhang Zhixu, Qi Yiquan et al. 2011. Simulations of the northern South China Sea using WAVEWATCH III and SWAN. Journal of Tropical Oceanography (in Chinese), 30(5): 27–37

Kiladis G N, van Loon H. 1988. The southern oscillation: Part VII. Meteorological anomalies over the Indian and Pacific sectors associated with the extremes of the oscillation. Monthly Weather Review, 116(1): 120–136

Li Chongyin. 1988. Actions of typhoons over the western pacific (including the South China Sea) and El Niño. Advances in Atmospheric Sciences, 5(1): 107–115

Lim Y K, Kim K Y. 2007. ENSO impact on the space-time evolution of the regional Asian summer monsoons. Journal of Climate, 20(11): 2397–2415

Meng Cuiling, Xu Zongxue. 2007. Relation between ENSO and precipitation in Shandong. Yellow River (in Chinese), 29(1): 33–35, 42

Mirzaei A, Tangang F, Juneng L, et al. 2013. Wave climate simulation for southern region of the South China Sea. Ocean Dynamics, 63(8): 961–977

Mirzaei A, Tangang F, Juneng L. 2014. Wave energy potential along the east coast of Peninsular Malaysia. Energy, 68: 722–734

Qi Yiquan, Shi Ping, Mao Qingwen. 1998. Characteristics of sea wave over the northern South China Sea from GEOSAT altimetric observations. Haiyang Xuebao (in Chinese) 20(2): 20–26

Qi Yiquan, Shi Ping, Mao Qingwen, et al. 1998. Analysis of typhoon Betty 1987 on sea surface wind and wave over the western Pacific using Geosat altimetric data. Haiyang Xuebao (in Chinese), 20(3): 27–35

Rogers W E, Kaihatu J M, Hsu L, et al. 2007. Forecasting and hindcasting waves with the SWAN model in the Southern California Bight. Coastal Engineering, 54(1): 1–15

Shi Neng, Zhou Jiade. 1990. Statistical analysis of relationship between typhoon activities over the northwestern Pacific and El Niño/Southern oscillation. Journal of Nanjing Institute of Meteorology (in Chinese), 13(3): 402–409

Stopa J E, Cheung K F, Tolman H L, et al. 2013. Patterns and cycles in the climate forecast system reanalysis wind and wave data. Ocean Modelling, 70: 207–220

Sun Chengzhi, Zhang Shengjun. 2007. The relationship between El Niño and the activity of typhoon in southeast China sea. Ocean Technology (in Chinese), 26(4): 94–97

Wan Yong, Zhang Jie, Meng Junmin, et al. 2015. A wave energy resource assessment in the China's seas based on multi-satellite merged radar altimeter data. Acta Oceanologica Sinica, 34(3): 115–124

Yaakob O, Hashim F E, Omar K M, et al. 2016. Satellite-based wave data and wave energy resource assessment for South China Sea. Renewable Energy, 88: 359–371

Yadav R K, Ramu D A, Dimri A P. 2013. On the relationship between ENSO patterns and winter precipitation over North and Central India. Global and Planetary Change, 107: 50–58

Yang Shengqiang, Hou Yijun, Liu Yahao. 2015. Observed typhoon wave spectrum in northern South China Sea. Chinese Journal of Oceanology and Limnology, 33(5): 1286–1294

Yu Mugeng. 1984. Analysing the characteristics of wave distribution in the south China sea on the basis of ship reports. Marine Science Bulletin (in Chinese), 3(4): 1–8

Yuan Yuan, Yang Hui, Li Chongyin. 2012. Study of El Niño events of different types and their potential impact on the following summer precipitation in China. Acta Meteorologica Sinica (in Chinese), 70(3): 467–478

Zheng Chongwei, Li Chongyin. 2015. Variation of the wave energy and significant wave height in the China Sea and adjacent waters. Renewable and Sustainable Energy Reviews, 43: 381–387

Zheng Chongwei, Pan Jing, Li Jiaxun. 2013. Assessing the China Sea wind energy and wave energy resources from 1988 to 2009. Ocean Engineering, 65: 39–48

Zheng Chongwei, Zheng Yuyan, Chen Hongchun. 2011. Research on wave energy resources in the northern south China sea during recent 10 years using SWAN wave model. Journal of Subtropical Resources and Environment (in Chinese), 6(2): 54–59

Zhou Liangming, Wu Lunyu, Guo Peifang, et al. 2007. Simulation and study of wave in South China Sea using WAVEWATCH-III. Journal of Tropical Oceanography (in Chinese), 26(5): 1–8

Zhuang Li. 1999. Characteristics of the wind and wave fields of typhoon over the northwest pacific. Meteorological Monthly (in Chinese), 24(7): 20–24